Optical scattering resonances of single and coupled dimer plasmonic nanoantennas

O. L. Muskens[1], V. Giannini[2], J. A. Sánchez-Gil[2], J. Gómez Rivas[1]

[1] *FOM Institute for Atomic and Molecular Physics AMOLF, c/o Philips Research, High Tech Campus 4, 5656 AE, Eindhoven, The Netherlands*
[2] *Instituto de Estructura de la Materia, Consejo Superior de Investigaciones Cientficas, Serrano 121, 28006 Madrid, Spain*

muskens@amolf.nl

Abstract: The optical resonances of individual plasmonic dimer antennas are investigated using confocal darkfield spectroscopy. Experiments on an array of antennas with varying arm lengths and interparticle gap sizes show large spectral shifts of the plasmon modes due to a combination of geometrical resonances and plasmon hybridization. The resonances of the coupled-dimer antennas are considerably broadened compared to those of single nanorods, which is attributed to a superradiant damping of the coupled antenna modes. The scattering spectra are compared with electrodynamic model calculations that demonstrate both the near-field and far-field characteristics of a half-wave antenna.

OCIS codes: (240.6680) Surface plasmons; (350.4990) Particles

References and links

1. U. Kreibig and M. Volmer, "Optical Properties of Metal Clusters," Springer Series in Material Science Vol. 25 (Springer-Verlag, Berlin, 1995).
2. D. Boyer, P. Tamarat, A. Maali, B. Lounis, and M. Orrit, "Photothermal Imaging of Nanometer-Sized Metal Particles Among Scatterers," Science **297,** 1160 (2002).
3. A. D. McFarland and R. P. van Duyne, "Single Silver Nanoparticles as Real-Time Optical Sensors with Zepto-mole Sensitivity," Nano Lett. **3**, 1057 (2003).
4. W. L. Barnes, A. Dereux, and T. W. Ebbesen, "Surface plasmon sub-wavelength optics," Nature **424**, 824 (2003).
5. T. A. Kelf, Y. Sugawara, J. J. Baumberg, M. Abdelsalam, and P. N. Bartlett, "Plasmonic Band Gaps and Trapped Plasmons on Nanostructured Metal Surfaces," Phys. Rev. Lett. **95**, 116802 (2005).
6. E. Ozbay, "Plasmonics: Merging Photonics and Electronics at Nanoscale Dimensions," Science **311**, 189 (2006).
7. J.C. Ashley and L.C. Emerson, 'Dispersion relations for non-radiative surface plasmons on cylinders,' Surf. Sci. **41**, 615 (1974).
8. J.-C. Weeber, A. Dereux, C. Girard, J. R. Krenn, and J.-P. Goudonnet, "Plasmon polaritons of metallic nanowires for controlling submicron propagation of light," Phys. Rev. B **60**, 9061 (1999).
9. J. R. Krenn, G. Schider, W. Rechberger, B. Lamprecht, A. Leitner, F. R. Aussenegg, and J. C. Weeber, "Design of multipolar plasmon excitations in silver nanoparticles," Appl. Phys. Lett. **77**(12), 3379 (2000).
10. K. Imura, T. Nagahara, and H. Okamoto, "Near-field optical imaging of plasmon modes in gold nanorods," J. Phys. Chem. B **108** 16344 (2004).
11. H. Ditlbacher, A. Hohenau, D. Wagner, U. Kreibig, M. Rogers, F. Hofer, F.R. Aussenegg, J.R. Krenn, "Silver Nanowires as Surface Plasmon Resonators," Phys. Rev. Lett. **95**, 257403 (2005)
12. J. Aizpurua, G. W. Bryant, L. J. Richter, F. J. García de Abajo, B. K. Kelley, and T. Mallouk, "Optical properties of coupled metallic nanorods for field-enhanced spectroscopy," Phys. Rev. B **71**, 235420 (2005).
13. P. Mühlschlegel, H.-J. Eisler, O. J. F. Martin, B. Hecht, and D. W. Pohl, "Resonant optical antennas," Science **308**, 1607 (2005).

14. P. J. Schuck, D. P. Fromm, A. Sundaramurthy, G. S. Kino, and W. E. Moerner, "Improving the Mismatch between Light and Nanoscale Objects with Gold Bowtie Nanoantennas," Phys. Rev. Lett. **94**, 017402 (2005).

15. J. N. Farahani, D. W. Pohl, H.-J. Eisler, and B. Hecht, "Single quantum dot coupled to a scanning optical antenna: a tunable superemitter," Phys. Rev. Lett. **95**, 017402 (2005).

16. R. M. Bakker, A. Boltasseva, Z. Liu, R. H. Pedersen, S. Gresillon, A. V. Kildishev, V. P. Drachev, and V. M. Shalaev, "Near-field excitation of nanoantenna resonance," Opt. Express **15,** 13682 (2007).

17. T. Taminiau, R. J. Moerland, F. B. Segerink, L. Kuipers, and N. F. van Hulst, "l/4 Resonance of an Optical Monopole Antenna probed by single molecule fluorescence," Nano Lett. **7**, 28 (2007).

18. O. L. Muskens, V. Giannini, J. A. Sánchez Gil, and J. Gómez Rivas, "Strong enhancement of the radiative decay rate of emitters by single plasmonic nanoantennas," Nano Lett. **7**, 2871 (2007).

19. C. F. Bohren and D. R. Huffman, *Absorption and scattering of light by small particles* (Wiley-VCH, 1998).

20. S. Link and M. A. El-Sayed, "Size and temperature dependence of the plasmon absorption of colloidal gold nanoparticles," J. Phys. Chem. B **103**, 8410 (1999).

21. C. Sönnichsen, T. Franzl, T. Wilk, G. von Plessen, J. Feldmann, O. Wilson, and P. Mulvaney, "Drastic reduction of plasmon damping in gold nanorods," Phys. Rev. Lett. **88**, 077402 (2002).

22. A. Brioude, X. C. Jiang, M. P. Pileni, "Optical Properites of gold nanorods:DDA simulations supported by experiments," J. Phys. Chem. B **109**, 13138 (2005).

23. S. W. Prescott, P. Mulvaney, "Gold Nanorod Extinction Spectra," J. Appl. Phys. **99,** 123504 (2006)

24. L. Novotny, "Effective wavelength scaling for optical antennas," Phys. Rev. Lett. **98**, 266802 (2007).

25. P. B. Johnson and R. W. Christy, "Optical Constants of the Noble Metals," Phys. Rev. B **6**, 4370 (1972).

26. T. Atay, J.-H. Song, and A. V. Nurmikko, "Strong interacting plasmon nanoparticle pairs: from dipole-dipole interaction to conductively coupled regime," Nano Lett. **4**, 1627 (2004).

27. L. Gunnarsson, T. Rindzevicius, J. Prikulis, B. Kasemo, M. Kll, S. Zou, and G. C. Schatz, "Confined plasmons in nanofabricated single silver particle pairs: experimental observations of strong interparticle interactions," J. Phys. Chem. B **109,** 1079, (2005).

28. I. Romero, J. Aizpurua, G. W. Bryant, and F. J. García de Abajo, "Optics in nearly touching metallic nanoparticles: singular response in the limit of touching dimers," Opt. Express **14** 9988 (2006).

29. T. Sondergaard and S. I. Bozhevolnyi, "Nano-strip Optical Resonators," Opt. Express **15,** 4198 (2007).

30. W. Rechberger, A. Hohenau, A. Leitner, J. R. Krenn, B. Lamprecht, and F. R. Aussenegg, "Optical properties. of two interacting gold nanoparticles," Opt. Commun. **220**, 137 (2003).

31. K.-H. Su, Q.-H. Wei, X. Zhang, J. J. Mock, D. R. Smith, and S. Schultz, "Interparticle coupling effects on plasmon resonances of nanogold particles," Nano Lett. **3**, 1087 (2003).

32. P. Nordlander, C. Oubre, E. Prodan, K. Li, and M.I. Stockman, "Plasmon hybridization in nanoparticle dimers," Nano Lett. **4**, 899 (2005).

33. J. P. Kottmann and O. J. F. Martin, "Retardation-induced plasmon resonances in coupled nanoparticles," Opt. Lett. **26**, 1096 (2001).

34. L. Allen and J. H. Eberly, *Optical Resonance and Two-Level Atoms* (General Publishing Company, 1987).

1. Introduction

The optical properties of small noble metal particles have been under investigation for many years [1]. Their optical response is governed by quasistatic oscillations of free electrons, which at characteristic frequencies in the visible give rise to a surface plasmon resonance. Small metal particles hold promise for many applications such as bio-labeling [2] and optical sensing [3]. On the other hand, surface plasmon polaritons on metal films are receiving attention for applications in optical data communication [4]. Between the limits of a small nanoparticle and a planar film, a surprisingly rich playground exists of complex plasmonic structures supporting either localized or propagating surface plasmon resonances, or a combination of both [5]. The mode spectrum of these complex plasmonic structures and their coupling to the radiation field is a topic of intensive theoretical and experimental studies [6].

The regime of polariton-like modes has been investigated for elongated metal nanorods, supporting higher order longitudinal resonances in the visible and near-infrared [7–12]. Due to their analogy with traditional radiowave antennas as convertor of electrical current to radiation, these resonant nanorods have recently been referred to as optical antennas [13,14]. By coupling two resonant structures to form a dimer, it was shown that nonlinear optical phenomena can be greatly enhanced [13–15]. Which antenna design is the most suitable for specific applications, like field enhancement [13, 14, 16] or light extraction [15, 17, 18], is a question of considerable

importance.

Here, we present a systematic study of the simultaneous effects of particle length and gap width in dimer antennas on the far-field optical resonances. By performing spectroscopy on individual nanoantenna structures, we gain access to the homogeneous spectral width of the antenna modes. Our experimental results are supported by electrodynamic model calculations using the Green function surface integral equations in parametric form. We emphasize at this point a controversy in the literature concerning the origin and physics of the splitting of the plasmonic mode spectrum for cylindrical nanorods. For many years, metal nanorods have been described as ellipsoids using quasistatic Mie-Gans theory [19–21]. For an ellipsoidal metal nanoparticle, spectral resonance positions depend purely on aspect ratio combined with the characteristic dispersion of the metal dielectric funtion with frequency. The Mie-Gans description has both been supported [22] and questioned [23] using numerical discrete-dipole-approximation modelling for cylindrical-shaped nanorods. A strong dependence of the longitudinal resonance position on both the nanorod width and the endcap morphology was found [23]. In the electrodynamic antenna description, resonances are purely geometrical [8–13, 24], and exist even for a perfect conductor. The confinement of plasmon polaritons inside the rod-like structure results in a non-trivial dependence of these spectral resonances on the length of the rod, on its radius, and on the finite permittivity at optical wavelengths [9, 10, 13, 24]. A precise understanding of plasmon resonances in this regime is of importance for many applications in nanophotonics.

2. Sample fabrication

Individual nanoantennas are fabricated using high-resolution electron-beam lithography. The substrate is a silicon wafer covered by a 500-nm layer of thermally grown silica. Nanoantennas were formed by deposition of a 20-nm gold film on the patterned surface followed by liftoff in acetone. Scanning electron microscopy (SEM) images of an array of nanoantennas are shown in Fig. 1(a), with magnified images of individual nanorods and dimer antennas numbered 1-4. In the array, the antenna arm length, L, is varied in the vertical direction, while the antenna gap width, Δ, is varied in the horizontal direction. The first column on the left contains single nanorods, as shown in images 1 and 2. The second column contains structures of two nanorods which are overlapping because the designed particle separation was too narrow for the liftoff process to succeed (image 3). The antennas with the smallest gaps have a separation Δ of 20 nm, as shown in image 4 of Fig. 1(a).

For further experiments, the structures were covered with a 20 nm thin dielectric layer consisting of a 10 nm sol-gel silica film and a 10 nm polyvinylbutanol layer. Together with the silica substrate, this results in a nearly homogeneous embedding of the antennas in a medium with a dielectric constant ε_m of ~ 2.25.

3. Experiments

The plasmonic modes of individual antennas are characterized by scattering spectroscopy using scanning confocal microscope in darkfield configuration. The illumination geometry consists of a cone of grazing-incidence wavevectors defined by the ~ 0.95 NA illumination ring. Scattered photons are collected by a $100\times$, 0.9 N.A. objective and detected, after confocal filtering, by an avalanche photodiode. Figure 1(b) shows the scattered intensities of individual antennas around a wavelength of 730 nm, for a polarization parallel to the antenna axes. The antenna with the highest intensity for each column in Fig. 1(b) is indicated by a red circle. Clearly, this maximum does not occur for the antennas with the largest particle size, indicating a resonance in the scattering cross section. For small gap widths $\Delta < 50$ nm, the maximum shifts to smaller arm lengths L. Antennas with arms that are overlapping do not scatter light at the selected wavelength since these can be considered as a single nanorod with resonances in the
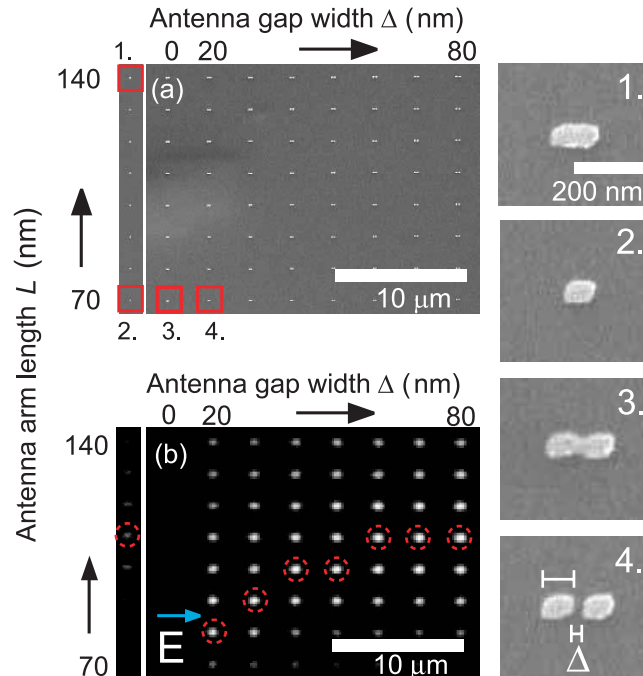
Fig. 1. (a) SEM image of a nanoantenna array with varied antenna arm lengths (vertical) and antenna gaps (horizontal), with detailed images of several single nanorods and dimer antennas. (b) Scattered intensity detected in a bandwidth of 730 nm $\pm$ 30 nm for polarizations parallel to the antenna long axes. (Circles, red) denote antennas with maximum scattering intensity for each of the columns with constant Δ.

infrared [26, 28].

A more detailed investigation was made by measuring the spectrally resolved scattered intensity of individual nanoantennas, using a spectrometer equipped with a high-sensivity CCD camera. Single-antenna spectra were integrated over 30 s and corrected for a background. To increase the signal quality, spectral channels were summed over a bandwidth of 5 nm. Figure 2(a-h) shows the resulting scattering spectra of single nanorods with lengths L varying between 70 nm and 140 nm, for polarization parallel (line, black) and perpendicular (dashed line, red) to the antenna long axis. The longitudinally polarized spectrum of Fig. 2(a) was normalized to its maximum, subsequently all other spectra, both longitudinal and transverse, were multiplied by the same amplitude scale factor, thus preserving the relative amplitude information. The two polarizations yield two different resonances corresponding to longitudinal and transverse modes of the nanorods. For the nearly square 70×60 nm^2 particle, the resonances are nearly degenerate. For nanorods with increasing lengths, the longitudinal mode shifts to longer wavelengths while the transverse resonance is unaffected. With a quality factor of around 7, the observed single-antenna resonances are considerably broader than those of chemically prepared nanorods in the quasistatic limit, where factors up to 25 have been reported [21]. Our results are reproduced by theoretical calculations [see Fig. 2(i-p)] as discussed below. We find reasonably good agreement in spectral resonance positions using the dielectric response function of gold from Ref. [25]. Similar to the experimental spectra, all vertical scales have been rescaled using an amplitude scale factor obtained from normalization of the maximum of the longitudinal mode of Fig. 2(i). Good agreement between experiment and calculation is obtained for
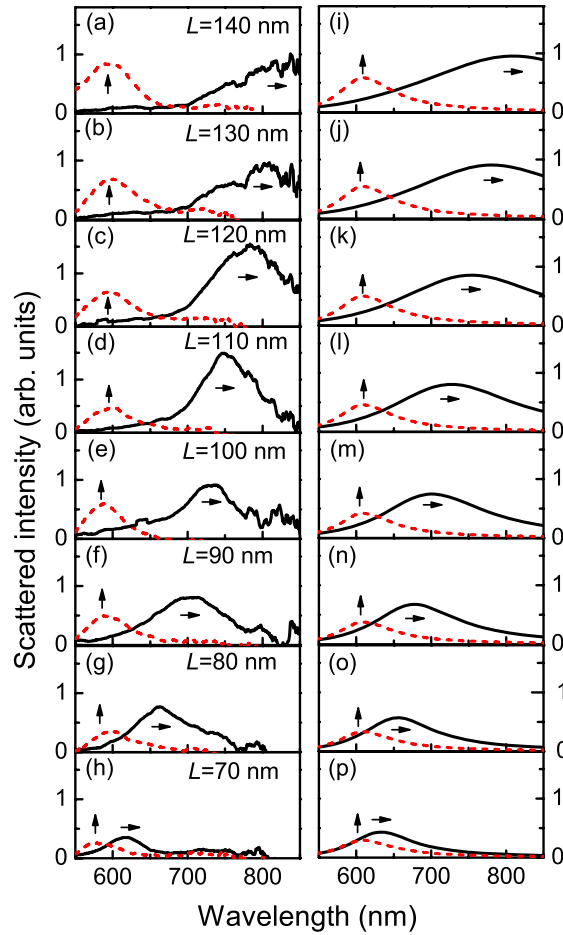
Fig. 2. (a-h) Experimental darkfield scattering spectra of individual gold nanorods with a width of 60 nm, height 20 nm, and lengths L varying from 70 nm to 140 nm for polarizations parallel (line, black) and perpendicular (dashed line, red) to the nanorod long axis. (i-p) Calculated scattering cross sections for longitudinal (line, black) and transverse (dashed line, red) polarizations. The vertical scales of the experimental and calculated spectra are normalized to the longitudinal modes of (a) and (i), respectively (see text).

the relative amplitudes of the longitudinal and transverse modes for each individual nanorod, as well as between the different nanorods.

Effects of arm coupling are investigated in Fig. 3(a-h), where we present the scattering spectra of dimer antennas with a gap Δ of 20 nm and arm lengths L between 70 nm and 140 nm. The spectra were rescaled vertically using the same amplitude scale factor as in Fig. 2(a-h). The longitudinal modes of the dimer antennas are redshifted by approximately 50 nm with respect to the modes of the single nanorods, and are considerably broadened by ∼50%, as is most clearly seen for the $L = 70$ nm antenna. For antenna lengths above $L = 110$ nm the spectral position of the longitudinal mode are located outside the experimentally accessible spectral window. For the dimer antennas we found larger particle-to-particle variations than for the single nanorods, which we attribute to enhanced sensitivity of the mode structure to small deviations in particle geometry and interparticle coupling. Theoretical calculations, shown in Fig. 3(i-p), are
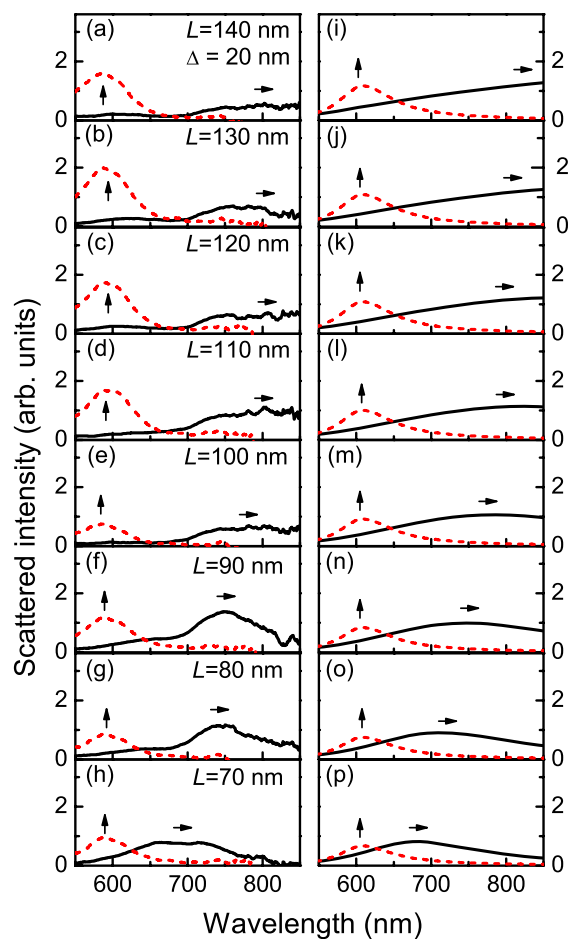
Fig. 3. (a-h) Experimental darkfield scattering spectra of dimer nanoantennas with an antenna gap Δ of 20 nm and arm lengths L varying from 70 nm to 140 nm. (i-p) Calculated scattering cross sections for longitudinal (line, black) and transverse (dashed line, red) polarizations. The vertical scales of experimental and calculated spectra are identical to those in Fig. 2(a-p).
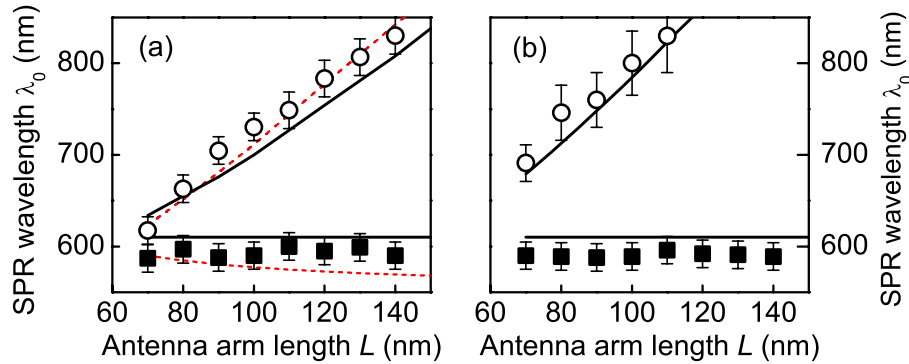
Fig. 4. Surface plasmon resonance wavelengths for (a) single nanorods and for (b) dimer antennas with a gap Δ of 20 nm, for longitudinal (open circles) and transverse (squares, black) polarizations. Solid black lines denote the resonances calculated using electrodynamical model calculations. Dashed red lines in (a) are the resonances calculated using the quasistatic Mie-Gans model for an ellipsoid. In all calculations $\varepsilon_m = 2.25$.

described further below. These calculations reproduce the overall general features of resonance shift and broadening, although some quantitative differences are clearly observed due to the mentioned experimental variations. Figures 4(a,b) show the spectral positions of the longitudinal (circles) and transverse (squares) modes against L for single nanorods [Fig. 4(a)] and for coupled dimer antennas [Fig. 4(b)].

4. Electrodynamic model calculations

To validate our experimental results, the plasmon modes of dimer nanoantennas are calculated using a scattering formalism based on Green's theorem surface integral equations in parametric form. For a rectangular parallelepiped illuminated along one of its principle axes, the induced components of the electric field are mostly located in the plane perpendicular to this axis along the polarization direction. Therefore, a rectangular rod can be approximated by a two-dimensional calculation [13, 29]. The corresponding 2D-geometries are a $20 \times L$ nm^2 rectangular slab for the longitudinal resonance, and a 20×60 nm^2 rectangular slab for the transverse resonance, as shown schematically by the configurations in Fig. 5. In both cases we assume incidence normal to the long axis of the effective 2D rectangle, with an electric field along the long axis. The lines in Figs. 2(i-p) show the calculated scattering cross sections for the cases corresponding to longitudinal (lines, black) and transverse (dashed lines, red) polarizations, for a dielectric constant of the surrounding medium $\varepsilon_m = 2.25$. The calculated resonance positions for different particle lengths are indicated by the black lines in Fig. 4. Note that in the calculations all the parameters are fixed; reasonably good agreement is obtained without fitting. For comparison we have also fitted the data using the quasistatic Mie-Gans model using an ellipsoid with dimensions of $60 \times 20 \times L$ nm^2 [c.f. red dashed lines in Fig. 4(a)]. The transverse resonance in this case shows a blueshift, caused by the coupling of the three depolarization ratios of the ellipsoid. Within the experimental error no frequency shift is observed for the transverse mode of the single nanorods [black squares in Fig. 4(a)]. However, the exact behavior will depend sensitively on slight variations in the metal dielectric function and the particle height, therefore no definitive conclusions can be drawn in this respect.

For the dimer antennas, the longitudinal resonance wavelengths [circles in Fig. 4(b)] show a continuous redshift with respect to the single-nanorod resonances, for all the antennas within
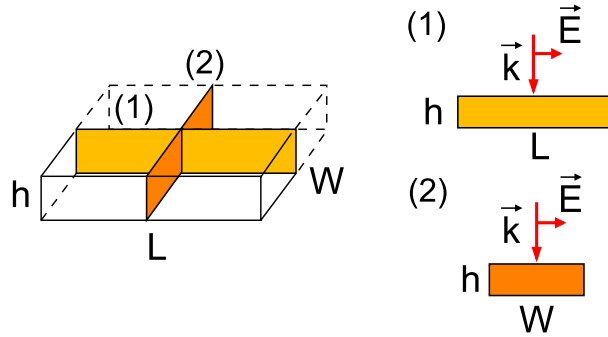
Fig. 5. Illustration of a three-dimensional nanorod with dimensions $L \times W \times h$, with respective two-dimensional systems 1 and 2 used in the calculation of scattering spectra for respectively longitudinal and transverse light polarizations.
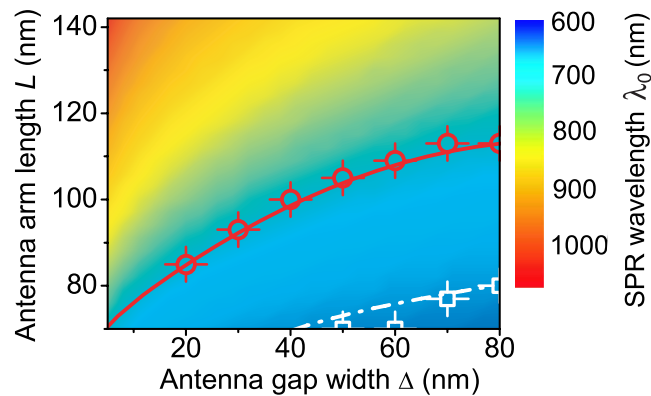

Fig. 6. Color density graph of calculated longitudinal antenna mode positions as a function of both antenna arm length L and antenna gap width Δ. (open circles, red) Positions of maximum intensity estimated from Fig. 1(b) as described in text, with (line, red) calculated isowavelength contour at $\lambda = 730$ nm. (squares and dashed line, white) same for $\lambda = 660$ nm.

the limited accessible spectral window. This is in quantitative agreement with our calculations [solid line in Fig. 4(b)] and with work on coupled rotation-symmetric rods supporting geometrical resonances [12]. Earlier experimental work on dimers has focused on cylindrical and elliptical (pillbox-shaped) particles with fixed aspect ratio [26, 27, 30, 31]. The spectral redshift of the longitudinal mode of interacting particles in general is well understood and has been described in terms of plasmon hybridization [32]. In contrast to cylinders [30, 33], we do not observe an orthogonal hybridization of the transverse mode. The strong broadening of the longitudinal mode for coupled particles is consistent with the superradiant damping of two coherently coupled, in-phase dipole oscillators.

Using the 2D scheme, the longitudinal mode spectrum has been calculated for all combinations of L and Δ of Fig. 1. Figure 6 shows the resulting longitudinal resonance positions. The red circles represent combinations (L,Δ) extracted from Fig. 1(b) for which an intensity maximum occurs at $\lambda = 730$ nm. This is done by interpolating the maximum of L from the data points at fixed value of Δ. The points follow well the calculated contour at $\lambda = 730$ nm, indicated by the red line. We also show results taken at $\lambda = 660$ nm (white squares). Figure 6 predicts well the
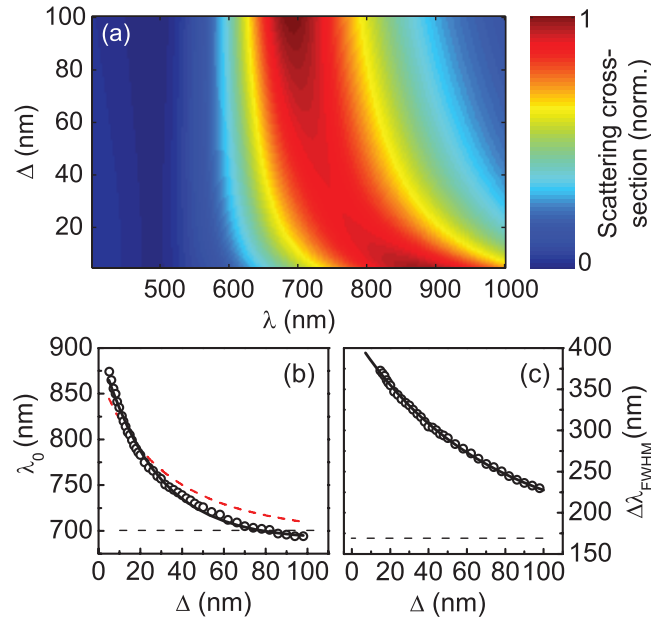
Fig. 7. (a) Color density graph showing the calculated scattering spectra for the $L = 100$ nm antenna and for longitudinal polarization, as a function of gap width Δ. (b) Spectral resonance position λ_0 and (c) full width-at-half maximum linewidth $\Delta\lambda_{\text{FWHM}}$ of the longitudinal mode of (a) against antenna gap width Δ, for (circles) electrodynamic calculations, and fits using (lines, black) exponential and (dashed line, red) dipole-dipole interactions. Horizontal dashed lines denote limiting values for single nanorod with $L = 100$ nm [c.f. Fig. 2(m)].

spectral resonance positions in a broad range of antenna parameters. Clearly many combinations of L and Δ result in the same spectral mode position. However, the near-field mode profile will depend strongly on the dimensions of the antenna gap [12, 13, 18].

A good illustration of the short range of the interaction between the two antenna arms is shown in Fig. 7(a). This is a cut through Fig. 6 showing the extinction spectra for a $L = 100$ nm dimer antenna as a function of the gap size Δ, normalized to the maximum at $\Delta = 100$ nm. The effect of particle coupling on the resonance wavelength increases steeply below $\Delta = 50$ nm. A small reduction of the resonance cross section of about 8% is observed around $\Delta = 40$ nm, of which we currently do not know the physical origin. The open circles in Figs. 7(b,c) show the calculated position and width of the plasmon resonance as a function of antenna gap size Δ. The values for the single nanorod, as extracted from Fig. 2(m), are indicated by the horizontal dashed lines in Fig. 7(b,c). The resonance wavelength λ_0 converges to that of the uncoupled antenna within $\Delta = 100$ nm, with a slight overshoot to the blue side due to the transition from the near-field to far-field coupling regimes [30]. We have fitted an exponential dependence on Δ of the resonance wavelength [thick line, black in Fig. 7(b)] and obtained a decay length of 23.7 ± 0.8 nm. A fit using the dipole-dipole $1/R^3$ interaction [dashed line, red in Fig. 7(b)] shows less good agreement with the full electrodynamic calculations, indicating that higher-order multipole interactions play a dominant role. The resonance width $\Delta\lambda_{\text{FWHM}}$ [c.f. Fig. 7(c)] converges much slower to its value for the uncoupled antenna with a decay length of 67.7 ± 0.5 nm, which we discuss below.

The exponential decay of the spectral resonance shift within tens of nanometers is consistent
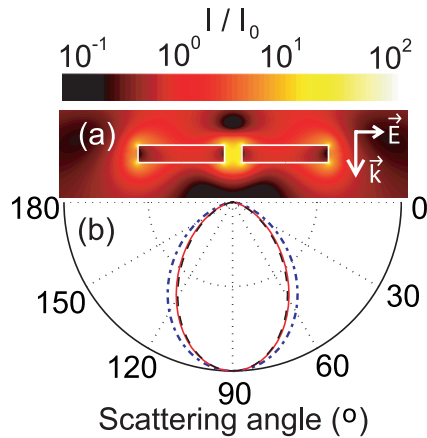
Fig. 8. (a) Near field intensity at the longitudinal resonance for an antenna with strongly coupled arms ($\Delta = 20$ nm, $L = 100$ nm). (b) Far-field scattering pattern of the antenna (solid line, red), together with the emission patterns of a point dipole (dash-dotted line, blue), and a half-wave antenna (dashed line, black).

with earlier observations [27, 31], and is representative for the short range of the interparticle coupling. The large difference in decay lengths between the spectral resonance shift and the linewidth indicates that the broadening does not only depend on the interparticle coupling. We have interpreted this broadening in terms of superradiance of the dimer antennas. Superradiance means that two in-phase oscillating dipoles loose their energy twice as fast due to the coherent addition of their dipole moments [34]. For the coupled antennas this coherence is induced by particle interactions. However, in the current configuration, the antenna arms are driven in-phase by the incident light field, both in the case of uncoupled and coupled antennas. The typical length scale over which two point dipoles add coherently without retardation is $\lambda_0/4$. This relation between the superradiance length scale and the optical wavelength may be modified for the extended charge distributions in the antennas. We find a 10% increase of the characteristic decay length of the resonance width with the interparticle separation when increasing the antenna size L from 70 nm to 110 nm (not shown), which correlates well with the corresponding shift of the plasmon resonance wavelength λ_0. This indicates a weak contribution of geometric effects on the superradiance length scale in the size regime under study.

As it is shown next, the coherent addition without retardation of the scattered intensity by the two arms of a nanoantenna should be differentiated from the breakdown of the quasistatic approximation for the plasmon resonance, which is a result of the strong reduction of the plasmon wavelength in the metal [12, 13, 17, 24]. The model calculations provide, next to the scattering cross-sections, also the optical near-fields and the far-field radiation pattern of the antenna. Figure 8(a) shows these for a strongly coupled antenna ($\Delta = 20$ nm, $L = 100$ nm) at resonance, for an incident plane wave as indicated in the figure. The intensity near-field enhancement (shown on a logarithmic scale) reaches 10^2 in the center of the antenna gap. Inside the antenna, the intensity drops to zero at the longitudinal edges of the arms, which is indicative of a half-wave resonance; a quasistatic mode would show a constant internal field. Further evidence of the non-validity of quasistatic models to describe the scattering by nanoantennas is obtained from the corresponding far-field emission pattern, shown in Fig. 8(b)(thick line, red). For comparison we plotted radiation patterns of a point dipole (dash-dotted line, blue), and a half-wave antenna (dashed line, black). Clearly, the antenna pattern corresponds to that of a half-wave dipole antenna, which has a more directional emission than a point dipole due to

interference of the radiation emitted over the total antenna length.

In conclusion, we have studied both experimentally and theoretically the scattering of single plasmonic nanoantennas. Darkfield spectroscopy showed a clear dependence of the longitudinal mode on antenna arm length and on gap width for dimers. We have used two-dimensional electrodynamical calculations using the Green's function surface integral equations to reproduce the experimental spectra. The observation of broad homogeneous resonance linewidths for the single antennas is consistent with strong superradiant damping. This radiative efficiency leads to efficient coupling of far-field light from a diffraction limited spot into a near-field mode volume [14]. Additionally, strong radiative damping may result in the suppression of ohmic losses, which in combination with the strong spatial mode confinement in the antenna gap may be extremely suitable for spontaneous emission enhancement of light emitters [18].